Proceedings of the 12th International Conference on
Aluminium Alloys, September 5-9, 2010, Yokohama, Japan

pp. 1690-1695

Evolution of the Nanostructure of a 7xxx Alloy During Retrogression and Re-ageing as Investigated by ASAXS and Atom Probe Tomography

Thorsten Marlaud[1,2], Alexis Deschamps[2], Williams Lefebvre[3]

[1]Rio Tinto Alcan - Centre de Recherches de Voreppe, BP 27, 38341 Voreppe Cedex, France

[2]SIMAP, INPGrenoble-CNRS-UJF, BP 75, 38402 St. Martin d'Hères CEDEX, France

[3]Groupe de Physique des Materiaux, CNRS – UMR 6634, Saint-Etienne du Rouvray, France

The technique known as retrogression and re-aging (RRA) is known to reduce the stress corrosion cracking susceptibility in 7XXX aluminium alloys, while keeping the strength levels similar to T6 temper. The RRA consists on a double aging, with a retrogression step between them. The first aging corresponds to the T6 temper and the retrogression consists on a partial anneal at temperatures usually between 180 and 240°C for times ranging from 5 to 2400 s, followed by a water quench. Finally, the alloy is re-aged at conditions similar to T6 temper. Very few data are available that give the accurate level of precipitate dissolution inside grain. Furthermore, very few attempts have been made to clearly characterize the nanostructure after RRA, mainly because the nanostructure is very complex. In the present work, we have combined Anomalous Small Angle X-ray scattering (ASAXS) and Atom Probe Tomography to describe in detail the evolution of solute distribution during retrogression and re-aging. Particular attention has been paid to the evolution of precipitate and matrix composition and to the fine-scale characterization of re-precipitation.

Keywords: *retrogression, re-aging, atom probe, SAXS*

1. Introduction

7000 series aluminium alloy are extensively used in aeronautical applications, due to their very high strength [1]. One limitation of their use in the metallurgical state of highest strength (commonly called T6 or T651 temper) is the low resistance to structural corrosion (stress corrosion cracking, exfoliation corrosion) (see for instance references [2-4]). Improving these properties to acceptable levels actually requires to overage the material to the expense of a ~30% loss of yield strength (T76 or T7651 temper). Such requirements become more and more demanding as solute contents are increased in commercial alloys in order to improve even further the mechanical properties.

In order to improve the compromise between mechanical strength and corrosion resistance, it has been proposed to replace the traditional 2-step heat treatment of these alloys by a three-step heat treatment, called retrogression and re-ageing treatment (RRA), which has been shown to offer a stress-corrosion resistance as good as that of a T76 heat treatment, while offering a strength comparable to that of a T6 temper (see for instance references [5]). This type of heat treatment comprises a first ageing step, leading to an under-aged or a T6 state. A second step (called retrogression or reversion), of short duration at high temperature, dissolves part of the initially formed precipitates. Finally, a third heat treatment step, at lower temperature, leads to the final microstructure.

The evolution of precipitate microstructures during the RRA treatments has been evaluated using a number of experimental techniques including small-angle X-ray scattering SAXS (see for instance [6]) mostly on classical aerospace alloys, such as AA7075, AA7150 or AA7449. A general view of the phenomena taking place has been obtained as follows :

- during the reversion step (performed usually on under-aged or peak-aged tempers) an initial diminution of hardness is observed, followed by a local maximum and a subsequent continuous decrease. The initial decrease is commonly interpreted as a dissolution of the initially present GP zones, and the local maximum as a transformation of the existing η' precipitates to the equilibrium

phase η. However the mechanisms depend on the initial temper of the material and the parameters of reversion (notably temperature), so that a complete picture is still missing.
- the re-aging step is interpreted in many different ways. Several mechanisms have been invoked in the literature, including the growth of partially dissolved η' precipitates, the re-nucleation of precipitates [7], the transformation to the stable η phase [8].

Though it is recognised that two of the main solute elements (namely Cu and Zn) show extensive substitution in the main hardening phase of this system (η'), very different diffusivity in the Al matrix [9] and an opposite effect on corrosion properties [10], no quantitative information is available on the influence of the RRA heat treatment on the distribution of solute between the nanoscale precipitates and the aluminium matrix.

We aim in this paper to provide a detailed, quantitative assessment of microstructure throughout the RRA heat treatment, which will address both the geometrical characteristics of precipitates (size, volume fraction, precipitate size distribution) and the chemistry of the precipitates and their counterpart (solid solution). This will be achieved by combining essentially two main experimental techniques, namely small-angle X-ray scattering (SAXS) and Atom-Probe Tomography (APT).

2. Experimental

2.1 Material and heat treatments

The present study was carried out on an alloy provided by Alcan Rio Tinto, of composition (in wt%) 10.3%Zn, 2%Mg, and 1.6%Cu (with minor additions of Zr and Sc to control grain size). The material was received as a 25 mm thick plate, subjected to a solution treatment at 471°C, followed by a water quench, 2% plastic deformation, and 6h of heat treatment at 120°C (heating ramp of 30°C/h). This state will be called PHT (partial heat treatment) in the following. Its hardness is almost as high as that of the T6 material, and it has a somewhat smaller precipitate size (precipitate radius of 18 Å vs. 32 Å). Reversion treatments have been carried out in an oil bath for the ex-situ measurements (APT, ASAXS, hardness) and in a rapid heating furnace (heating rate 10°C/s) for the in-situ SAXS experiments. It was tested on selected samples that the two heating procedures did not induce significant changes in the microstructures. Although different RRA conditions have been studied in the present work (time and temperature of reversion step), the reference heat treatment that will be used when not stated otherwise is 20 minutes at 185°C. Re-ageing heat treatments were carried out similarly to the initial partial heat treatment, namely 6h at 120°C with a heating rate of 30°C/h. They were started immediately after the reversion step in order to avoid natural ageing between the two steps. The retrogression and re-aged (RRA) material was compared to a material subjected to a model peak-ageing (PA) treatment, consisting of a water quench from a solution treatment at 470°C, 4 days at room temperature, a first ageing step of 22h at 120°C with a ramp speed of $30°C.h^{-1}$, and a second step of 8h at 150°C with a ramp speed of $15°C.h^{-1}$.

2.2 Atom Probe Tomography (APT)

For APT analyses, 0.3 x 0.3 x 20 mm^3 blanks were cut from the plates and prepared into needles by standard electropolishing in 2% perchloric acid (70%) in 2-butoxyethanol at 15 V at room temperature. Atom Probe analyses were carried out with an apparatus of type ECOTAP and TAP both equipped with the same detection system. Analyses were performed at 10^{-8} Pa with a pulse fraction of 19% and a pulse repetition rate of 2.0 kHz. The tip temperature was set to 40 K, which does not lead to any preferential evaporation of Mg in Al [11]. Data analyses were conducted using the software developed in the University of Rouen and the maximum separation distance method [12] was applied to identify clusters and precipitates.

2.3 Small-Angle X-ray Scattering (SAXS)

SAXS experiments were carried out on two different apparatus. First, all in-situ experiments during the second and third steps of the RRA treatment were carried out on a laboratory set-up using a rotating anode with a Cu K_α source. The beam, of wavelength 1.54 Å, was focused and conditioned by a multi-layer mirror, and traversed a sample of thickness ~70 µm. The scattering was collected by a CCD camera located at 50 cm from the sample, giving access to the range in scattering vectors [0.015, 0.3 $Å^{-1}$]. The data was corrected for electronic noise, pixel efficiency, geometrical artefacts, and background noise, and then carefully normalized using beam monitoring.

The evaluation of the precipitate size was done in several ways. First, the Guinier radius was calculated in a similar way as in [13], to provide a simple measurement of precipitate size. A more complete analysis was conducted on some scattering curves making the assumption that the precipitates consist of ellipsoids of revolution following a log normal distribution. The scattering signal of such distributions, assuming no interference between particles (low volume fraction limit), can be calculated exactly if one assumes a random orientation of the particles with respect to the X-ray beam (see e.g. [14]). A non linear fitting procedure was used to obtain the three parameters of the precipitate distribution from the experimental data (namely average size, relative distribution width and precipitate aspect ratio). The volume fraction was calculated classically using the integrated intensity, and the precipitate number density was calculated from the volume fraction and size of precipitates. Anomalous SAXS (ASAXS) experiments were carried out on the European synchrotron source in Grenoble (ESRF) on the BM02-D2AM beamline. A monochromatic beam of diameter ~200 µm was used, with an energy dispersion of $\delta E/E \sim 2.\ 10^{-4}$. Two absorption edges were used, namely the Zn and Cu K_α edges, with six different energies for each case. Measurements were carried out in the same conditions on three reference samples (all containing precipitates), used to calibrate precisely the evolution of the diffusion factors with beam energy: a binary Al-Zn alloy, a binary Al-Cu alloy, and a binary Al-Li sample showing no anomalous effect. Precipitate composition was evaluated using the same procedure as in [13], assuming that the precipitates consist only of a phase with a composition of $Mg(Al,Zn,Mg)_2$, and a constant Al content of 15 at%. Matrix compositions were calculated using a mass balance with the alloy composition, using the volume fraction of precipitates and the precipitate compositions.

3. Atom Probe Tomography evaluation of the microstructure in the reference peak aged temper and in the RRA temper

APT reconstructions of the reference peak-aged temper (PA) and the reference retrogression and re-aged temper (RRA) indicate that the RRA treatment, while showing comparable precipitates as compared to the PA treatment, leads to a significantly different solute distribution in between precipitates. While the matrix in the PA treatment is characterised by an apparently uniform dispersion of solute, the RRA treatment shown evident fluctuations of the solute distribution. For the RRA treatment, the regions between precipitates cannot be simply considered as a matrix with a higher solute content, in contrast with the PA treatment. We will assume from now that, after the RRA treatment, the nano-structure is composed of a matrix, precipitates and solute rich clusters that differ from precipitates. These clusters will now be studied in some detail.

To distinguish each of these three types of regions in APT datasets, it has been decided to apply the maximum separation distance algorithm [12] (hereafter designated as MSD), since it has been proved to be very powerful for the analysis of very small clusters (about 10 atoms or more). With this algorithm, solute atoms are gathered in a cluster if their separation distance is less than a distance hereafter called d_{max}. Then, only clusters containing more than N_{min} atoms are considered. The well known drawbacks of this method are: i) the difficulty in determining the accurate combination of parameters d_{max} and N_{min}; ii) the unavoidable selection of artificial clusters due to statistical fluctuation in the matrix.

In the present work, we have determined the best compromise best set of N_{min} and d_{max} parameters according to a heuristic procedure based on the comparison with an equivalent randomised APT data set. This procedure set of parameters for the MSD algorithm: d_{max} = 0.5 nm and N_{min} =10. From now, the clusters and precipitates selected in APT analyses are identified with the MSD algorithm according to these input parameters. One should however keep in mind that although "artificial" clusters may still be selected, their proportion to the "real" clusters is minimised.

Figure 1 shows the precipitates and clusters detected for the RRA and PA treatments respectively. Well-defined precipitates are present after both treatments. However, more clusters are present in between precipitates for the RRA treatment. Size distributions have shown that particles either contain much less than 500 atoms or much more. This threshold has hence been used to distinguish clusters from precipitates. The C_{Zn}/C_{Cu} ratio between Zn and Cu atom fractions has been calculated for clusters and precipitates (Table 1). In precipitates, this ratio is significantly lower for the RRA treatment compared to the ratio observed for the PA treatment. On the contrary, in clusters, the C_{Zn}/C_{Cu} ratio is much larger in the RRA volumes than in the PA volumes. It is also noticeable that for the RRA treatment, the C_{Zn}/C_{Cu} ratio is much larger in clusters than in precipitates. The opposite trend is observed in the PA treatment. One should however notice that the ratio calculated for the PA clusters is close to the solute ratio in the alloy (7.2 vs. 6.6). This suggests that the clusters detected in the PA treatment are likely to correspond to the noise of the MSD algorithm, and correspond actually to random fluctuations of the solid solution.

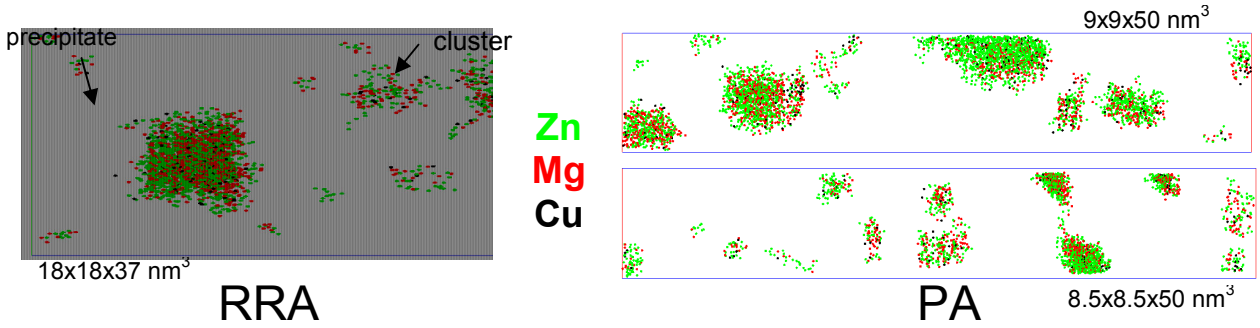

Fig. 1: Clusters and precipitates identified by the MSD algorithm in the RRA and PA treatments.

C_{Zn}/C_{Cu}	PA	RRA
Clusters	7.2	19.5
Precipitates	12.4	8.8

Table 1 : C_{Zn}/C_{Cu} (at. %) ratio as determined by APT in clusters (i.e. containing less than 500 atoms) and precipitates (i.e. particles containing more than 500 atoms).

The matrix and cluster compositions have been calculated and reported in Table 2. The matrix concentration has been simply calculated by removing clusters and precipitates from analysed volumes. It appears that the matrix concentration in Zn and Cu is roughly the same for the PA and RRA treatments, whereas the Mg concentration is much larger for the RRA treatment. Furthermore, it is noticeable that the clusters formed during the RRA treatment display a C_{Zn}/C_{Mg} ratio of 2.

		Clusters composition				Matrix composition			
		Al	Zn	Mg	Cu	Al	Zn	Mg	Cu
PA	**content (at%)**	**75.7**	**13.7**	**8.7**	**1.9**	**95.55**	**3.29**	**0.71**	**0.44**
	standard deviation	0.5	0.5	0.4	0.2	0.05	0.04	0.02	0.02
RRA	**content (at%)**	**80.1**	**12.8**	**6.4**	**0.7**	**94.78**	**3.32**	**1.51**	**0.39**
	standard deviation	0.4	0.3	0.4	0.1	0.06	0.03	0.02	0.01

Table 2 : Matrix and clusters composition as determined by APT in the PA and RRA states respectively. The matrix composition was deduced by simply removing clusters and precipitates identified by the MSD algorithm. Clusters contain less than 500 atoms.

3. Evolution of precipitate microstructures during the different steps of the RRA heat treatment

3.1 Kinetics of precipitate evolution during the reversion step at 185°C

We first present in figure 2 the evolution of the precipitate volume fraction, Guinier radius and number density as well as the hardness during reversion at 185°C from the initial temper (PHT). The evolution of the microstructure parameters is similar to what has been found several times in the literature [15-16].

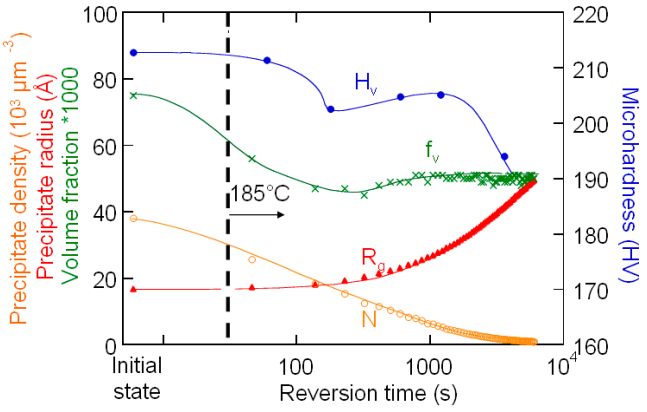

Fig. 2 : Evolution of Precipitate size, volume fraction and number density (measured in-situ by SAXS) and of Vickers microhardness (measured ex-situ after oil bath treatments) during reversion at 185°C, carried out from a PHT initial state.

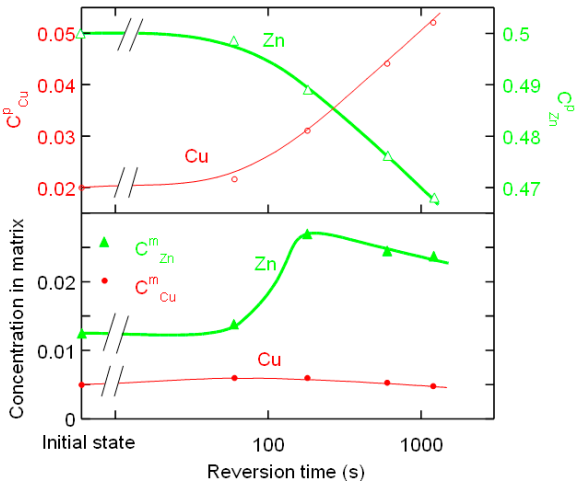

Fig. 3 : Evolution of precipitate and matrix concentrations (atomic) in Cu and Zn, as calculated from the ASAXS data, during reversion at 185°C.

Namely, three stages can be distinguished:

- a stage of rapid dissolution of precipitates (decrease of volume fraction and precipitate density), where the average precipitate size stays constant. This rapid dissolution is due to the destabilization of the precipitates initially present in the microstructure due to the temperature increase (the critical size for precipitate dissolution becoming much larger than the size of all precipitates), and the fact that the radius of precipitates is constant results from the combination of the slower dissolution rate of large precipitates as compared to small ones, and the disappearance of small precipitates in the solid solution;
- a stage of increase of the volume fraction, where the precipitate size increases as well, and the precipitate density continues to decrease. This stage is actually a coarsening stage, and the increase of volume fraction towards its equilibrium value is due to the lesser importance of the Gibbs Thomson effect when the precipitates grow in size;
- a stage of constant volume fraction, where the precipitate size continues to increase, with a corresponding decrease of precipitate density. This stage is the classical coarsening stage, when the material is close to equilibrium at the temperature of the reversion step (185°C).

3.2 Evolution of precipitate composition during reversion

Using ASAXS, we have evaluated the precipitate and matrix composition evolution during the reversion treatment at 185°C. The results are shown in figure 3. Initially, the precipitates are relatively rich in Zn and have a low Cu concentration (about 2 at%). It is observed that this concentration increases dramatically during the reversion treatment and reaches more than 5 at% after 20 min at 185°C, with a corresponding decrease of the Zn concentration since the two species are substituted in the same phase. The consequence on the matrix concentration is also very interesting.

The evolution of precipitate compositions, together with that of the precipitate volume fraction, results in a constant Cu matrix content, accompanied by a rising Zn matrix content that doubles during the reversion treatment.

4. Conclusion

Using a combination of complementary experimental techniques, and principally Atom Probe Tomography and Anomalous Small Angle X-ray Scattering, we have evaluated the mechanisms that prevail in the different stages of the retrogression and re-ageing (RRA) treatment, which can now be compared to that of more traditional peak-aged (PA) heat treatments. RRA and PA tempers have similar hardness, but very different microstructures. PA material shows a distribution of precipitates with an average size close to 3 nm, whereas the RRA material has in addition a dense distribution of very small clusters, containing less than 500 atoms. The distribution of solute is also very different, and the RRA temper shows precipitates richer in Cu (except clusters), and a matrix richer in Zn.

A complete evaluation of the kinetics of precipitate evolution during the different steps of the RRA treatment shows that the reversion step consists in a strong decrease of the precipitate volume fraction with a limited increase in precipitate size. The extra solute provided to the aluminium matrix consists almost only of Zn, leaving the remaining precipitates with a high Cu concentration. This behaviour is explained by the difference in solute diffusivity of Cu and Zn, together with the miscibility of these elements in the precipitates. During the re-ageing stage of the RRA heat treatment, the nucleation of new particles is observed. The chemistry of precipitates continues to evolve. Their Cu composition remains higher than that of the PA temper, a well as the Zn concentration of the solid solution.

References

[1] T. Warner: Materials science forum 519-521(2006)1271-1278.
[2] D. Adenis, A. Guilhaudis : Mémoire scientifiques revue métallurgique64 (1967) 877-889.
[3] P.N. Adler, R. De Iasi, G. Geschwind : Metallurgical transactions3 (1971) 3191-3200.
[4] W. Gruhl: Aluminium54 (1978) 323-325.
[5] W. Wallace, J. Beddoes, M. de Malherbe : Canadian aeronautics and space journal 27 (1981) 223-332.
[7] J.K. Park, A.J. Ardell : Metallurgical transactions a 15A (1984) 1531-1543.
[8] F. Viana, A.M. Pinto, H.M. Santos: Journal of materials processing technology 92-93 (1999) 54-59.
[9] H. Bakker, H.P. Bonzel, C.M. Bruff, M.A. Dayananda, W. Gust, J. Horvth, I. Kaur, G. Kidson, A.D. LeClaire, H. Mehrer, G. Murch, G.Neumann, N. Stolica, N.A. Stolwijk: *Diffusion in Solid Metals and Alloys.* Springer Verlag, (1990).
[10] E.H. Hollingsworth, H.Y. Hunsicker: Corrosion of aluminum and aluminum alloy. In: Corrosion Handbook. (1987).
[11] F. Danoix, M.K. Miller, A. Bigot: Ultramicroscopy 89 (2001) 177-188.
[12] J.M. Hyde: D.Phil Thesis, Oxford, (1993).
[13] T. Marlaud, A. Deschamps, F. Bley, W. Lefebvre, B. Baroux: Acta materialia 58 (2010) 248-260.
[14] F. Perrard, A. Deschamps, F. Bley, P. Donnadieu, P. Maugis: Journal of applied crystallography 39 (2006) 473-482.
[15] B. Gueffroy, H. Löffler: Physica status solidi (a) 66 (1981) 585-590.
[16] M. Nicolas, A. Deschamps: Acta materialia 51 (2003) 6077-6094.